Astron. Astrophys. 339, 467–476 (1998)

ASTRONOMY
AND
ASTROPHYSICS

Physical parameters of the Keplerian protoplanetary disk of DM Tauri

Stéphane Guilloteau and Anne Dutrey

Institut de Radio Astronomie Millimétrique, 300 Rue de la Piscine, F-38406 Saint Martin d'Hères, France

Received 22 June 1998 / Accepted 24 August 1998

Abstract. We present high sensitivity $3''$ aperture synthesis images of the DM Tau protoplanetary disk in the ^{12}CO J $= 1 \rightarrow 0$ line. The images unambiguously reveal that the disk is rotating around the central star. To model the observations in terms of a rotating disk in hydrostatic equilibrium, we have developped a χ^2 fitting procedure which allows derivation of the disk parameters and their errors. Dependencies among the disk parameters are discussed in detail. The disk is large, with an outer radius of 850 AU. We find that the rotation curve is essentially Keplerian, at least up to 600 AU. The stellar mass derived from the rotation curve is $0.50 \pm 0.06\,\mathrm{M}_\odot (D/150\,\mathrm{pc})$. The intrinsic local velocity dispersion in the disk is found to be essentially thermal, with a turbulent component of less than 30 % of the thermal width. Parameters derived from this observation are used to confirm the molecular abundances and depletion factors estimated for several simple organic molecules by Dutrey et al (1997) for DM Tau.

Key words: stars: individual: DM Tau – circumstellar matter – stars: pre-main sequence – radio-lines: stars

1. Introduction

Because of its location in a hole of the Taurus molecular complex, the relatively old (5 10^6 yr) low mass T Tauri star DM Tau has recently become a key object in the study of protoplanetary disks. Circumstellar gas was discovered by Guilloteau & Dutrey (1994, hereafter GD94) with the IRAM 30-m telescope. The line profiles obtained from ^{12}CO J $= 2 \rightarrow 1$ and ^{13}CO J $= 2 \rightarrow 1$ were consistent with a disk inclined about 30° from face-on, in Keplerian rotation around a $\simeq 0.65\,\mathrm{M}_\odot$ central star (GD94). Simple organic molecules like CN, HCN, CS, H_2CO, HCO^+ and HNC have also been discovered towards DM Tau by Dutrey, Guilloteau and Guélin (1997, DGG97), and have allowed the first estimate of a disk mass independent from the dust properties, as well as absolute molecular depletions. Interferometric observations of ^{12}CO with $\simeq 5''$ resolution performed by Saito et al (1995) confirmed the existence of a velocity gradient along an axis at PA $\sim 160^\circ$.

Send offprint requests to: S.Guilloteau
Correspondence to: guillote@iram.fr

These results make DM Tau the best known example of a proto solar system. However, because of the limited angular resolution, the evidence for rotation (and for the disk aspect) is indirect. Similar line profiles could in principle be produced by an infalling flattened envelope. Indeed, Saito et al (1995) found the CO emission to be marginaly elongated with a major axis at PA $\sim 57^\circ$, i.e. perpendicular to the velocity gradient axis, which would rather suggest infall than rotation.

So far, rotation around T Tauri stars has been demonstrated only for GM Aur (Koerner et al 1993, Dutrey et al 1998), another "old" (2 10^6 yr) T Tauri star. On the other hand, infall motions have been advocated for very young, presumably protostellar, objects such as B335 (Zhou et al 1993), L1527 (Myers et al 1995) or L1157 (Gueth et al 1997). Infall motions have been also invoked for the young star HL Tau by Hayashi et al (1993) while Sargent & Beckwith (1991) suggested that the disk was in Keplerian rotation, but these results have been questioned by Cabrit et al (1996) because of the confusion with the molecular outflow edges. Since only relatively old T Tauri stars have been shown to exhibit rotating disks, it suggests that Keplerian rotation may be established relatively late during the pre main sequence evolution of T Tauri stars. In this respect, establishing unambiguously whether DM Tau is dominated by rotation or by infall is important.

Moreover, mm arrays now offer the possibility to detect and *resolve* the CO emission of circumstellar disks around nearby PMS stars (see e.g. Koerner and Sargent 1995). It is then reasonable to start quantitative analysis of interferometric maps by χ^2 fitting using classical disk models.

We thus performed CO J $= 1 \rightarrow 0$ interferometric observations of the DM Tau disk and compare them to disk models using a standard χ^2 method. We study the possible interferometric biases, the influences of the various parameters on the model and their dependencies. We then focus on the measurement accuracy of some fundamental parameters such as the velocity law and the central mass.

2. Observations

We observed the ^{12}CO J $= 1 \rightarrow 0$ line and 2.7 mm continuum between Sep.3 and Oct.20 1995 with the IRAM Plateau de Bure 4-antenna interferometer. The typical precipitable wa-

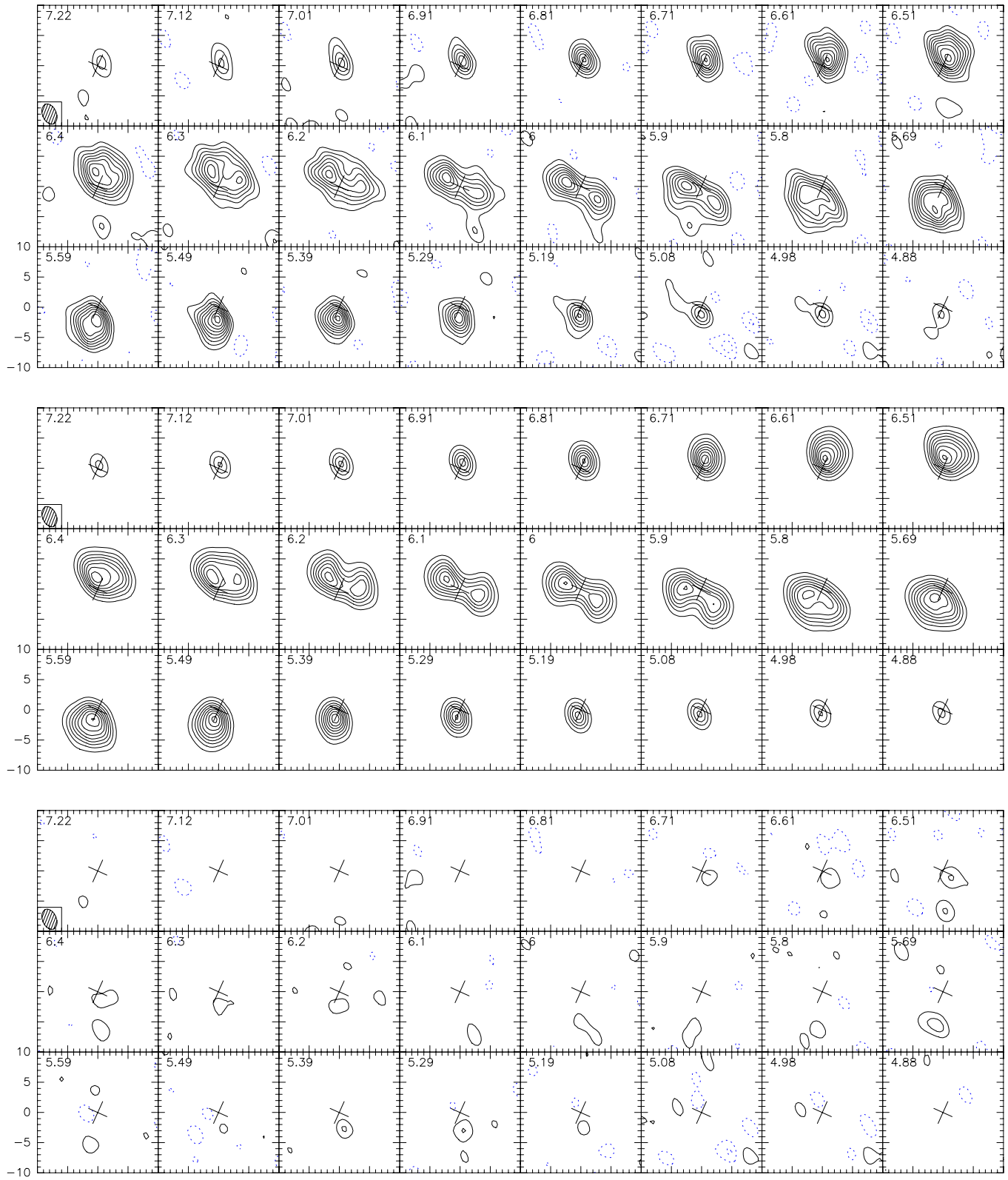

Fig. 1. Top: Channel map of the ^{12}CO J $= 1 \rightarrow 0$ toward DM Tau. The angular resolution is $3.5 \times 2.4''$ at PA 24°. Coordinates are offsets in $''$ from the continuum position, R.A. $04^h\ 33^m\ 48.735^s$ Dec. $18°10'10.2''$ (J2000.0). Contour spacing is 80 mJy/beam, or 0.9 K (2 σ). The LSR velocity is indicated in each panel. The cross indicates the position of the continuum source, and the orientation of the disk axis. Middle: best model, with same contour levels. Bottom: difference between observations and best model.

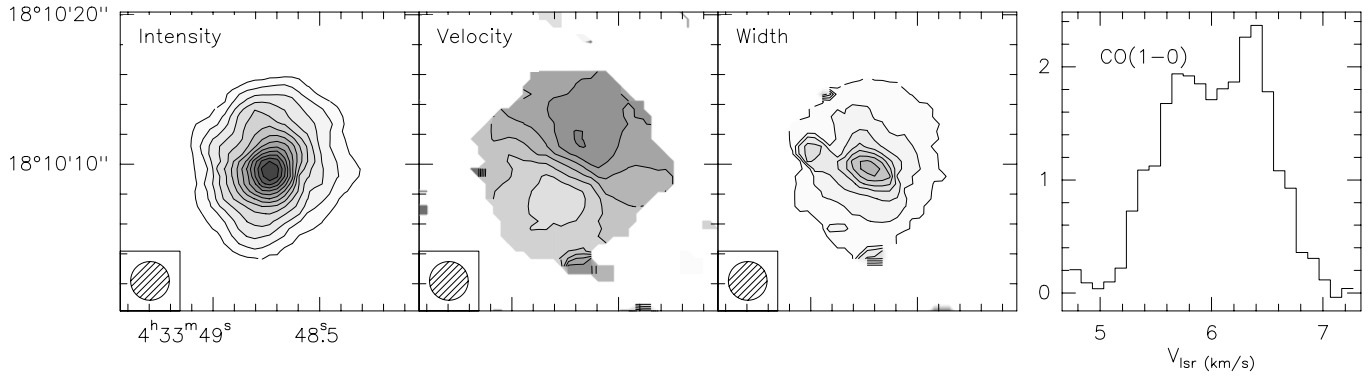

Fig. 2. Montage of the integrated intensity of the ^{12}CO J $= 1 \rightarrow 0$ map (contour levels from 50 to 700 by 50 mJy/beam. km s^{-1}) the velocity field (contour levels 5.8 to 6.6 by 0.2 km s^{-1}), the line width (contour levels 0.2 to 1.2 by 0.2 km s^{-1}), the integrated spectrum (in Jy) towards DM Tau. Uniformly weighted images restored with a circular beam of 2.6″ were used to derive these results.

ter vapor content was between 2.5 and 4.5 mm. The observing frequency was 115.3 GHz in the upper sideband and 112.3 GHz in the lower sideband. SIS mixers were tuned to provide a 6dB sideband rejection, offering system temperatures around 300 K. Three configurations with baselines from 24 to 176 m provided an angular resolution of $3.5 \times 2.3''$ at PA 24°. Phase and amplitude calibrations were performed on the nearby quasar 0528+134 whose flux density was 5.4 Jy during the period of the observations, based on flux monitoring performed at IRAM. Phase noise was between 10 and 25 degrees. One correlator unit provided 160 channels of 39 kHz separation (0.1 km s^{-1}); the effective resolution is about 65 kHz or 0.17 km s^{-1}. A second correlator with a total bandwidth of 160 MHz was used to provide continuum information.

Fig. 1 presents channel maps of the ^{12}CO J $= 1 \rightarrow 0$ emission line towards DM Tau. Integrated intensity, velocity field and line width maps are displayed in Fig. 2, together with the integrated spectrum. Fig. 1 also present images expected for the Keplerian disk model discussed in Sects. 4-5.

3. Results and analysis of interferometric biases

The maps of DM Tau presented in Figs. 1-2 are strikingly similar to what is expected from a protoplanetary disk in rotation around DM Tau. The double-peaked line profile (Fig. 2) and the "peanut" shape at the systemic velocity (near 6 km s^{-1}, Fig. 1) are two characteristic features of disks which are easily identified in DM Tau. Neither of them allows to disentangle between rotation or infall, however. Evidence for *rotation* is given by Fig. 2b, which shows that the velocity gradient is along the major axis of the integrated emission, while it would be expected along the minor axis if infall motions dominate, and tilted and skewed in the intermediate mixed case of infall + rotation. We point out, however, that the use of a velocity pattern derived with an elliptical beam would produce a distortion of the velocity field which could easily be mistaken for a combination of infall and rotation. This is illustrated in Fig. 3, where we compare the same Keplerian model restored with elliptical and circular beams, respectively. To analyse the velocity field, it is thus essential to use a circular pattern, as we did in Fig. 2, or to compare with a model restored with the same beam as the observations. Velocity gradients in marginally resolved objects may otherwise be severely distorted.

Ideally, one would also like to confirm that the major axis derived from the CO emission is identical to that derived from the continuum emission, as in GG Tau (Dutrey et al 1994, hereafter DGS94) or in GM Aur (Dutrey et al 1998). The centroid of the continuum emission (indicated by a cross in Figs. 1-2) is located at R.A. $04^h33^m48.735^s$ Dec. $18°10'10.2''$ (J2000.0). Its total flux is 18.1 ± 1.9 mJy, consistent with the ~ 110 mJy 1.3 mm bolometer flux measured by Beckwith et al (1990) for dust emission with a spectral index $\beta \simeq 1$. The continuum source is unfortunately too weak to measure any significant elongation, although a circular Gaussian fit to the UV data gives an (intrinsic) size of $0.9 \pm 0.4''$.

The outer disk radius is at least $6''$ (see Fig. 1-2), or $>$ 750 AU. This value is in agreement with the estimate from GD94, but much larger than the ~ 350 AU derived by Saito et al (1995). This is most likely due to the increased sensitivity of our observations which allow to trace out weak emission at larger distances from the star. Indeed, because of the difficulty to deconvolve weak extended structure, interferometric images always underestimate the outer size and total flux. An analysis in the UV plane is required to avoid this bias.

Fig. 1 also shows a direct comparison with a more elaborate disk model, described in details in Sects. 4-5, which clearly demonstrates that such a model provides an essentially perfect representation of the data.

4. Disk models

To better quantify the parameters of the DM Tau disk given in Sect. 5.3, we have performed a χ^2 analysis based on a "standard" rotating disk model.

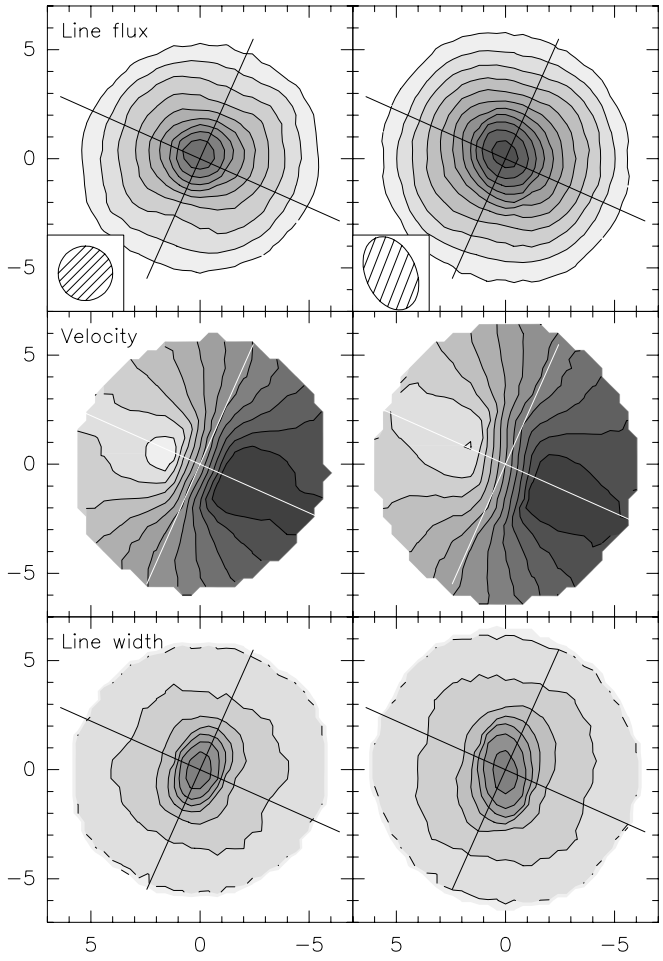

Fig. 3. Influence of the restoring beam on the apparent velocity gradient, for the same Keplerian model (best DM Tau model, but tilted to PA -24°, see Sect. 4). Left: uniformly weighted images restored with a circular beam of $2.5''$. Right: naturally weighted images restored with an elliptical beam of $3.5'' \times 2.3''$ with PA = 24°. Note how the isovelocity and linewidth contours appear skewed in the right panels. This could be mistaken for a combination of infall + rotation.

4.1. Model description and properties

We used the disk model described in DGS94 for GG Tau. The disk parameters are: the center position (x_0, y_0), the position angle PA and inclination i of the disk rotation axis along the line of sight ($i = 0$ means the disk is face on), the disk systemic velocity $V_{\rm LSR}$, the disk radius $R_{\rm out}$, the temperature $T(r) = T_0 r^{-q}$, the surface density $\Sigma(r) = \Sigma_0 r^{-p}$, the rotation velocity $V(r) = r^{-v}$. We assume the gas is in hydrostatic equilibrium: the scale height is $H(r) = H_0 r^h$ with $h = 1 + v - q/2$, and the density is $n(r) = n_0 r^{-s}$ with $s = p + 1 + v - q/2$. We also assume the linewidth δV (1/e half width) has a turbulent component dV in addition to the thermal line width $V_{th}(r) = \sqrt{2kT(r)/m}$; we will note ΔV the full width at half maximum:

$$\begin{aligned}\Delta V(r) &= 2\sqrt{ln(2)}\,\delta V(r) \\ &= 2\sqrt{ln(2)}\,\sqrt{\frac{2kT(r)}{m} + (dV(r))^2} \end{aligned} \quad (1)$$

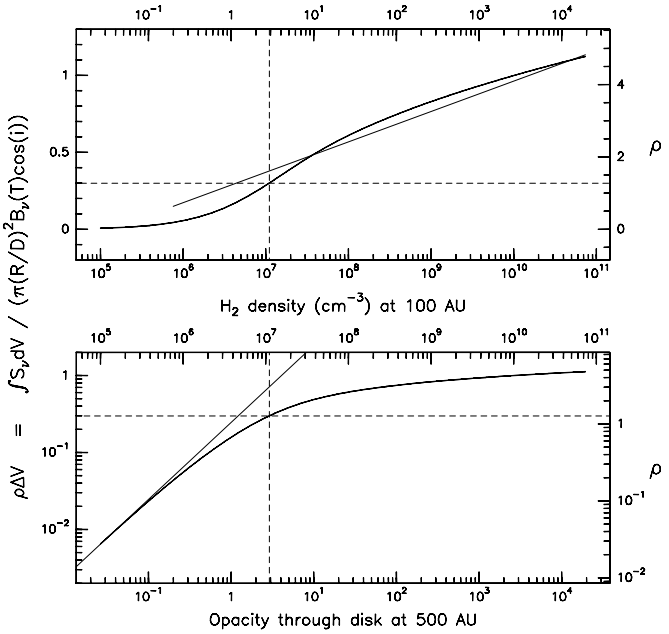

Fig. 4. Factors $\rho\Delta V$ (i.e. integrated line flux density S_ν divided by the optically thick flux) versus line opacity through the disk at 500 AU. The corresponding density scale n_0 is computed for the ^{12}CO J $= 1 \rightarrow 0$ line parameters, assuming an abundance of $1.4\,10^{-5}$ for CO.

Such a disk model has *a priori* 13 free parameters $(x_0, y_0, PA, i, R_{\rm out}, V_{\rm LSR}, T_0, q, V_0, v, \Sigma_0, p, dV)$. The position (x_0, y_0) can be accurately determined from the continuum (dust) emission. With 11 free parameters, and a computing time for a single model of order 1 to 2 minutes, a general χ^2 fitting would require a prohibitive time. It is thus essential to recognize *a priori* the dependencies between the various parameters.

Our approach is the following. We first show the *a priori* dependencies between the parameters derived from the integrated line flux expression. We then assume the rotation law is Keplerian, and analyse the importance of the dependencies using 2-parameter fits for several pairs of parameters (see Fig. 5a–c and 6a–f). The final parameter determination is done considering the minimum set of strongly coupled parameters (Fig. 7a–c). Finally, we assess the validity of the Keplerian rotation curve (Fig. 8).

To understand the dependencies among the various disk parameters, it is convenient to start from a formal expression of the integrated line flux. Assuming for simplicity a uniform temperature disk ($q = 0$), the integrated line flux can be written as

$$S_\nu = B_\nu(T_0)(\rho\Delta V)\pi R_{\rm out}^2/D^2\cos(i) \quad (2)$$

where D is the distance (we neglect the influence of an inner radius R_i, since this is typically $\sim 0.1 - 1$ AU). Eq. 2 holds because the emitting area at any given velocity is proportional to the local linewidth ΔV (see Beckwith and Sargent 1993), while $B_\nu(T_0)$ is the surface brightness and $\pi R_{\rm out}^2/D^2\cos(i)$ the projected area of the disk. The quantity ρ is a factor which includes all "hidden" dependencies. ρ obviously depends on the

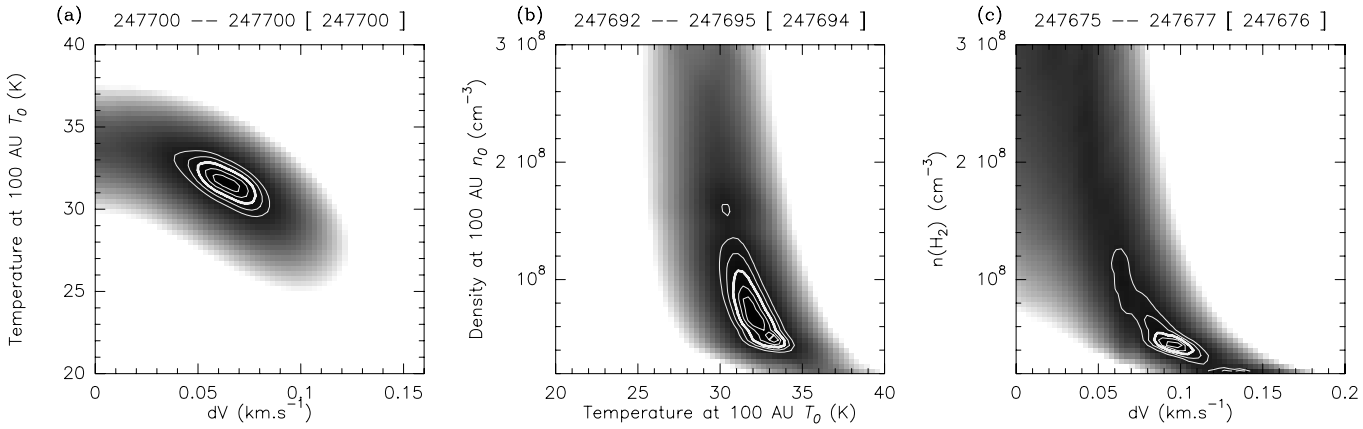

Fig. 5a–c. χ^2 analysis of the DM Tau disk. Iso-χ^2 surfaces for (T_0, dV) (n_0, T_0) and (n_0, dV), with all other parameters fixed to the values given in Table 1. Isocontours correspond to the 1 to 6 σ errors, with the 3σ contour enhanced. The greyscale runs from 1 to 16 σ. The numbers given above each panel are (from left to right): the interpolated minimum, the minimum on the original grid, and between brackets the adopted minimum to define the contours.

line opacity τ. For optically thin lines, ρ is $\propto \tau$, hence to the surface density Σ_0. For optically thick lines, ρ continues to increase with Σ_0, although more slowly. This occurs because the effective line width still depends on the line opacity, roughly as $ln(\tau)$ for gaussian profiles. ρ also depends on the inclination i, Eq. 2 being only valid for moderate inclinations ($\leq 70°$), because for nearly edge-on disks, the details of the vertical structure of the disks dominate the line-of-sight opacity distribution.

The dependency implied in Eq. 2 is clearly shown in Fig. 4 where we plot the integrated density flux S_ν (or more precisely the value of $\rho \Delta V$ as defined in Eq. 2) as a function of increasing density n_0. For this figure, the temperature law is $T_0 = 20$ K and $q = 0$, and all other model parameters are as in Table 1. With these parameters, the effective line width is constant: $\Delta V = 0.23\,\mathrm{km\,s^{-1}}$. The linear regime corresponds to $\tau << 1$ with the transition to the non-linear case occuring around $\tau \sim 1$.

Fig. 4 can also be used to determine the effective value of the ρ factor as a function of line opacity. This will be discussed in Sect. 6.3. Eq. 2 demonstrates the strong couplings in the $(T_0, dV, R_{\rm out}, i, \Sigma_0)$ set when only integrated values are available.

4.2. χ^2 definition

For each set of parameters, we compute the brightness distribution of the J $= 1 \rightarrow 0$ line of ^{12}CO as a function of the line of sight velocity assuming LTE as described in DGS94. The LTE hypothesis is justified by the low critical density of the ^{12}CO J $= 1 \rightarrow 0$ line. A synthetic UV data set is then computed from the model image using the same UV coverage (including weights) as for the observations.

The χ^2 distance between a model and the observations is:

$$\chi^2 = \Sigma_n \Sigma_i (Re(mod_{i,n}) - Re(obs_{i,n}))^2 \times W_i + \Sigma_n \Sigma_i (Im(mod_{i,n}) - Im(obs_{i,n}))^2 \times W_i \quad (3)$$

where $Re(a)$ (resp $Im(a)$) is the real (resp. imaginary) part of visibility a, and $a_{i,n}$ is the visibility i for velocity channel n. The weight W_i is derived from the system temperature T_{sys}, spectral resolution $\Delta\nu$ and integration time τ, including correction for the digitization noise introduced by the correlator efficiency η :

$$W_i = \frac{1}{\sigma_i^2} \ \text{with} \ \sigma_i = \frac{\sqrt{2} k T_{sys}}{A_{eff} \eta \sqrt{\tau \Delta\nu}} \quad (4)$$

where A_{eff} is the effective collecting area of one antenna. The χ^2 is defined directly from the UV plane data to avoid several problems in the map plane interpretation, such as non-linear effects in the deconvolution, number of independent measurements, noise correlation between adjacent pixels, etc... We have checked that the reduced χ^2 ($\chi^2/(2N_cN_v)$, where N_c is the number of channels and N_v the number of visibilities) is extremely close to 1 near the minimum, as expected for a large number of measurements.

The model is a discrete approximation of a continuous distribution over 2 dimensions of space and 1 of velocity. Physically, the observations provide the (frequency) integrated brightness distribution in each velocity channel. Proper comparison between the model and the observations thus requires i) a sufficiently fine spatial sampling, so that the sampled values are a good representation of the mean value over each pixel, ii) a proper integration in the frequency domain if the intrinsic spectral line width is small compared to the channel width. Basic models were computed with a spatial grid of 64×64, running over $3 \times R_{\rm out}$. Hence the typical pixel size is about $0.20''$, much smaller than the synthesized beam. In velocity, we should *in principle* integrate over very fine spectral channels to mimick the observing procedure. We have checked in practice that the results are not significantly different when using directly the observed velocity sampling of $\simeq 0.10\,\mathrm{km\,s^{-1}}$.

4.3. Density dependence

Since the ^{12}CO J $= 1 \rightarrow 0$ transition is easily thermalized and optically thick, we expect that the dependence on density n_0 will be relatively weak. This behaviour is illustrated in Fig. 5a–c,

Table 1. DM Tau: parameters of the model fit. 1) parameter name, 2) symbol, 3) value used for fixed parameters in Fig. 5-8, 4) best value and errorbar. All errors are formal 2 σ errors from the χ^2 analysis. If no error is given, the parameter is not properly constrained by the available data. The error on the velocity exponent is an estimate, since only a 2-parameter fit was done in this case. Note that PA is the position angle of the rotation axis of the disk.

(1)	(2)	(3)	(4)
Distance	D	150	150 pc
Systemic velocity	$V_{\rm LSR}$	6.05	6.05 ± 0.02 km.s^{-1}
Orientation	PA	66	$65 \pm 2^\circ$
Inclination	i	33	$33 \pm 3^\circ$
Outer radius	$R_{\rm out}$	850	850 ± 20 AU
Turbulent width	dV	0.07	$0.05 < dV < 0.11\,{\rm km\,s^{-1}}$
Temperature law: $T(r) = T_{100}(\frac{r}{100{\rm AU}})^{-q}$			
Temperature at 100 AU	T_{100}	31.5	32 ± 2 K
temperature exponent	q	0.62	0.63 ± 0.05
Density law : $n(r) = n_{100}(\frac{r}{100{\rm AU}})^{-s}$			
Density at 100 AU	n_{100}	10^8	$1\,10^8$ cm^{-3}
density exponent	s	2.75	2.75
Velocity law: $V(r) = V_{100}(\frac{r}{100{\rm AU}})^{-v}$			
V sin(i)	$V_{100}\sin(i)$	1.14	1.14 ± 0.03 km.s^{-1}
velocity at 100 AU	V_{100}	2.10	2.10 ± 0.15 km.s^{-1}
velocity exponent	v	0.5	$0.57 \pm \sim 0.04$
Centrifugal radius	R_c	$> R_{\rm out}$	630 ± 70 AU

provided the density at 100 AU exceeds $\sim 10^8{\rm cm}^{-3}$. At lower densities, when the lines become partly optically thin, the best fit is obtained for $n_0\Delta V = Constant$ as expected from Eq. 2. Although the best fit seem to appear for densities $\simeq 4\,10^7$ cm^{-3}, we caution that this result is most likely an artefact due to the large CO line opacities and the assumption of sharp edges for the disk. Since in practice, the disk probably does not have sharp edges, the minimization tries to mimic smooth edges by having an opacity < 1 at the disk edge. Except for this problem, the χ^2 is essentially uniform along the "valley" of best parameters in Fig. 5c. Fig. 5a–c shows that T_0 can be quite accurately determined, despite the dependency between T_0, n_0 and dV. The turbulent line width dV, which is constrained by the extent of the emission in each velocity channel, is dependent on the assumed density, but a safe upper limit of $\sim 0.1\,{\rm km\,s^{-1}}$ can be set.

4.4. Geometric parameters

Neglecting the slight dependency on density, and using the best value for the line width $dV = 0.07\,{\rm km\,s^{-1}}$, we are thus left with 8 free parameters. The disk orientation PA and systemic velocity $V_{\rm LSR}$ can be quite accurately determined from the channel maps. Assuming Keplerian rotation ($v = 0.5$) further reduces the coupled set to 5 parameters: $(T_0, q, R_{\rm out}, i)$ and the rotation velocity V_0. (V_0, i) are so tightly coupled that it is more convenient to select $(V_0\sin(i), i)$ as an independent set of parameters to explore the χ^2 hypersurface.

The coupling between these 5 parameters occurs only through the finite angular resolution. A strong coupling occurs beween $(T_0, q, R_{\rm out}, i)$: for example, a smaller value of $R_{\rm out}$ can be compensated by a smaller value of i. Similarly, a steeper temperature law (larger q) will tend to produce lower inclinations i. However, the disk inclination is not only constrained by the aspect ratio of the disk, but also by the kinematic pattern. This is because, in rotating disks, the locii of constant projected velocities are curves depending on $(V_0\sin(i), v, i)$. Variations in q only displace the maximum of brightness along the isovelocity curves, without changing their shapes. We thus may hope that the inclination i can be determined accurately despite the existing coupling between $(T_0, q, R_{\rm out}, i)$.

These behaviours are illustrated in Fig. 6a–f which represents several 2-D cuts through the χ^2 hypersurface. Note that in Fig. 5a–c and 6a–f, the minima obtained for various pairs of parameters do not coincide exactly: typical differences are about 4, i.e. 2 σ. This is a combination of two effects due to the finite step in our computations. First, the optimum parameters are only bracketted by the set of values used for the computations. Second, for each pair of parameters, the χ^2 surface is computed on a rough grid (typically 7×7), which is then re-interpolated on a finer 64×64 grid to produce the contour and greyscales plots. The observed differences in minimal χ^2 values are the result of limited resolution for some parameters. The original

step size for each parameter must be smaller than its formal 1σ error, but in case of strongly coupled parameters, a finer grid is required: this can be clearly seen in Fig. 6a–f and for the (T_0, q) plane (see Fig. 5a–c) which shows very narrow minima.

Given this uncertainty, we will only quote 2 σ formal errors in the subsequent numerical results, but use the 1 σ spacing for the χ^2 contours in Fig. 5-8.

5. Consequences of the disk modelling and χ^2 fit

5.1. Application to DM Tau

We computed models for DM Tau assuming a distance $D = 150\,$pc. The H_2 density law was $n(r) = 1\,10^8 (r/100\,\mathrm{AU})^{2.75} \mathrm{cm}^{-3}$. For ^{12}CO, we assumed a depletion factor of 5, i.e. an abundance of $1.4\,10^{-5}$, as derived by DGG97. The choice of these values will only affect the effective line width, since the $^{12}\mathrm{CO\,J} = 1 \rightarrow 0$ line is optically thick throughout the disk in this case (see Sect. 4.3 and Fig. 5a–c). This density was chosen in order to match the ^{12}CO, ^{13}CO and $\mathrm{C^{18}O\,J} = 2 \rightarrow 1$ lines observed at the 30-m by DGG97. With this density law, the disk mass is still $\simeq 2-3$ times smaller than that derived from the millimeter flux densities assuming a dust emissivity of $\kappa(\nu) = 0.1(\nu/10^{12}\mathrm{Hz})^{\beta}$ (see Beckwith et al 1990, Dutrey et al 1996, DGG97).

The analysis presented above shows that $(T_0, q, R_{\rm out}, V_0 \sin(i), i)$ are inter-dependent, and that an exponent of order $q = 0.6$ may be best for the temperature law. We thus performed a full 4-parameter fit for $(T_0, R_{\rm out}, V_0 \sin(i), i)$ for 3 different values of q: 0.5, 0.625, and 0.75. A $6 \times 6 \times 5 \times 6$ grid was used. For each value of q, a $\chi^2(T_0, R_{\rm out}, V_0 \sin(i), i)$ surface is computed; the $\chi^2(R_{\rm out}, V_0 \sin(i), i)$ surface is derived by parabolic interpolation along T_0 using only the 3 best χ^2 for each set of $(R_{\rm out}, V_0 \sin(i), i)$. The procedure is repeated along $R_{\rm out}$ to derive the $\chi^2(V_0 \sin(i), i)$ surfaces plotted in Fig. 7a–c. $q = 0.625$ does give a significantly better fit, $q = 0.5$ and $q = 0.75$ being at the 5σ level. A similar procedure was applied to derive the $\chi^2(R_{\rm out}, T_0)$ surface; we actually found that $R_{\rm out}$ is independent of all other parameters.

Best fit values and 2 σ errorbars are given in Table 1. Synthetic images for the best fit model are given in Fig. 1, and the difference between the best fit model and the observations is plotted in Fig. 1. In Fig. 1, it can be seen that the brightness distribution is not symmetric about the major axis, as would be expected since the disk is symmetric about its mid-plane. This is due to a self-absorption effect in a thick (or flared) disk. The farthest part appears brighter than the closest part of the disk, because of projection effects and decreasing temperature outwards. This self-absorption feature allows to recover the full 3-D orientation of the disk. The best solution is obtained the north-eastern part farther from the observer than the south-western part of the disk and an inclination of 33°, significantly better (6 σ) than the opposite with a slightly lower inclination ($-27°$).

5.2. The rotation law

So far, we have assumed the rotation law was Keplerian. Using all other parameters as in Table 1, Fig. 8a shows that rotation velocity is decreasing with radius with a best exponent $v = 0.57 \pm 0.04$. This is slightly steeper than expected for Keplerian rotation. A possible explanation is the existence of a centrifugal radius R_c beyond which the rotation is no longer Keplerian, but the rotation velocity falls faster with r, e.g. r^{-1}, or is zero. Fig. 8b shows that R_c may be of order $630 \pm 70\,$AU. This may indicate that Keplerian rotation has not yet been established up to the outer edge of the disk. However, most importantly, the rotation velocity at 100 AU (i.e. the derived stellar mass) is hardly affected in such case. Confirmation of such an effect would require higher angular resolution.

6. Discussion

6.1. Disk structure

Our results demonstrate that the temperature falls off approximately as r^{-q} with $q = 0.63 \pm 0.05$, a value consistent with heating by starlight in a thick flared disk, but excluding the "classical" value expected for an active accretion disk (or a passive thin disk), $q = 0.75$ at the 5σ level.

An interesting result which can be seen from Fig. 6e is that the turbulent component of the line width must be very small, of order $dV = 0.07\,\mathrm{km\,s^{-1}}$. This value applies essentially to the outer disk ($R > 200\mathrm{AU}$). We also considered the case where the turbulent line width is a constant *fraction* f of the thermal line width: $f = dV(r)/V_{th}(r)$ (see Fig. 6f).

In this case, the turbulent component is about $0.2-0.3$ times the thermal width. Such low turbulent widths provide additional support for the hypothesis of hydrostatic equilibrium for the vertical density structure, at least in the outer disk.

6.2. Stellar mass

In Sect. 5.2, we also demonstrate that despite the uncertainty in the shape of the rotation law, the velocity V_0 can be used to determine the dynamical mass of the system, i.e. the stellar mass if the inner disk mass is small. Assuming Keplerian rotation, we obtain $V_0 \sin(i) = 1.14 \pm 0.03\,\mathrm{km\,s^{-1}}$ at 100 AU, but V_0 is much less accurately determined because of the uncertainty in the inclination. Taking into account the slight correlation between $V \sin(i)$ and i (see Fig. 7b), the "best" value is $V_0 = 2.10 \pm 0.15\,\mathrm{km\,s^{-1}}$, corresponding to a stellar mass of $M = 0.50 \pm 0.06 M_{\odot}$, where the uncertainty is dominated by the error on the inclination i. This is somewhat lower than the 0.65 $M_{\odot}$ derived using the evolutionary tracks of Mazitelli (1989). In such a comparison, we should also consider the errors due to the distance uncertainty in both determinations. The mass derived from the rotation velocity is strictly proportional to the distance D, while the mass derived from the evolutionary tracks has a shallower dependance (because the measured luminosity scales with D^2 while the stellar luminosity varies with M^3 to M^4,

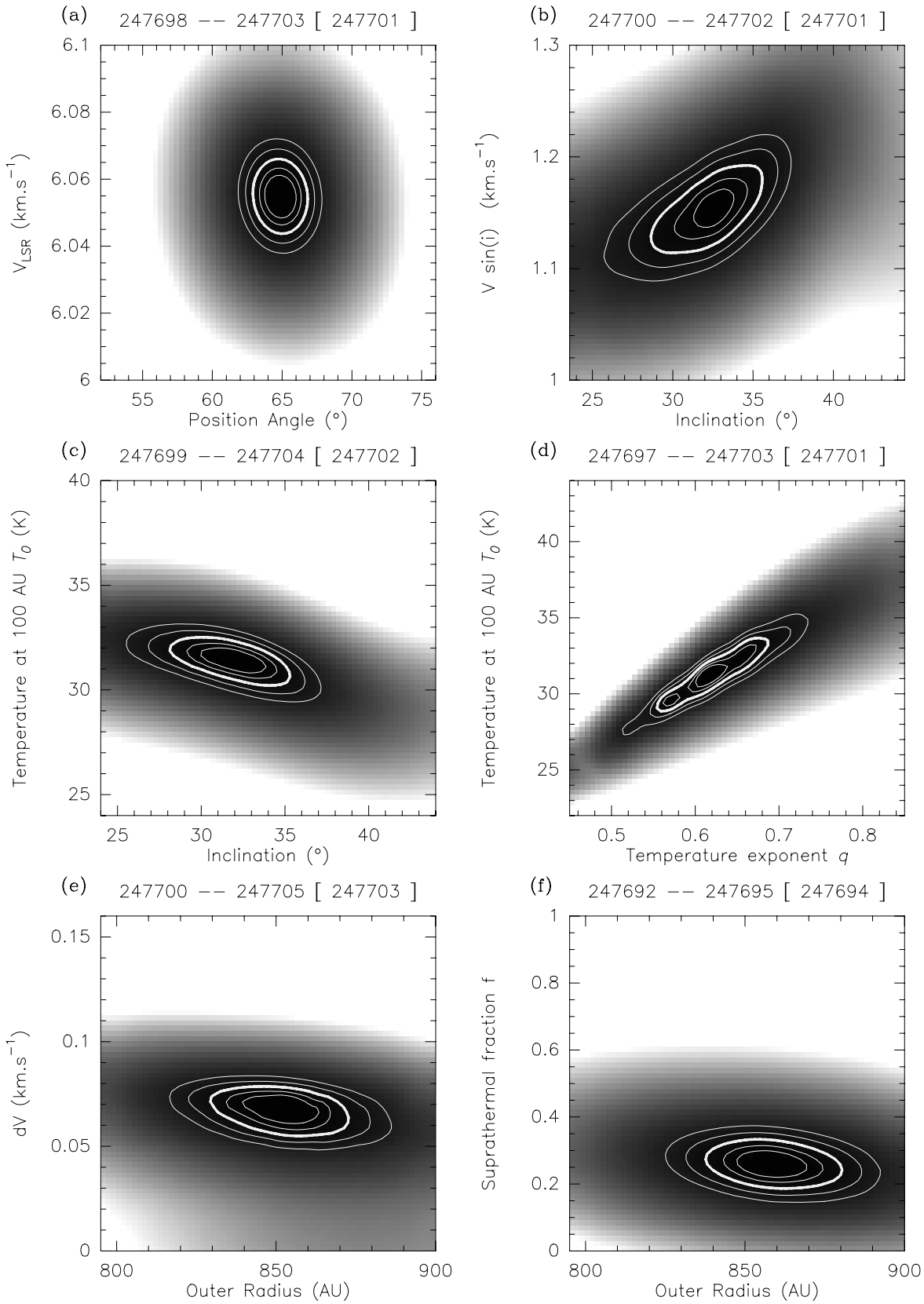

Fig. 6a–f. Results of the χ^2 analysis of the DM Tau disk. The images are iso-χ^2 surfaces for 2 parameters, with all other parameters were fixed to value given in Table 1. Presented surfaces are: **a** ($PA, V_{\rm LSR}$), **b** ($i, V_0 \sin(i)$), **c** (T_0, i), **d** (T_0, q), **e** ($R_{\rm out}, dV$) with fixed dV, and **f** ($R_{\rm out}, f$) where f is the ratio of turbulent width over the thermal line width ($f = dV(r)/V_{th}(r)$, i.e. the total line width is $\delta V(r) = (1+f)V_{th}(r)$). Isocontours correspond to the 1 to 5 σ errors.

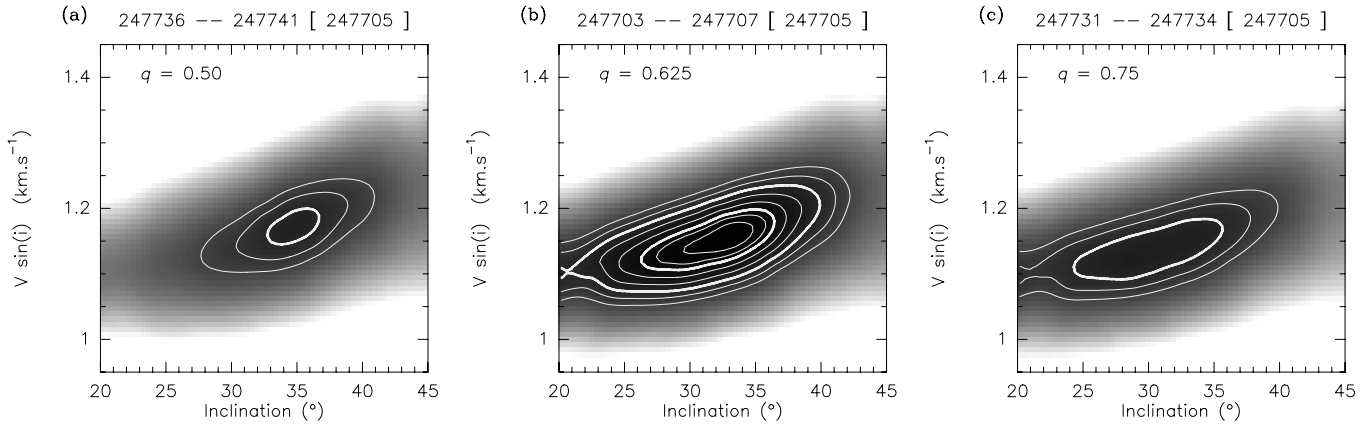

Fig. 7a–c. χ^2 analysis of the DM Tau disk. Iso-χ^2 surfaces for $(V_0 \sin(i), i)$ for 3 different values of q. Parameters $R_{\rm out}, T_0$ are optimally adjusted for all values of V_0, i; all other parameters fixed to the values given in Table 1. Isocontours correspond to the 1 to 8 σ errors, with the 3 and 6σ contours enhanced. The greyscale runs from 1 to 16 σ.

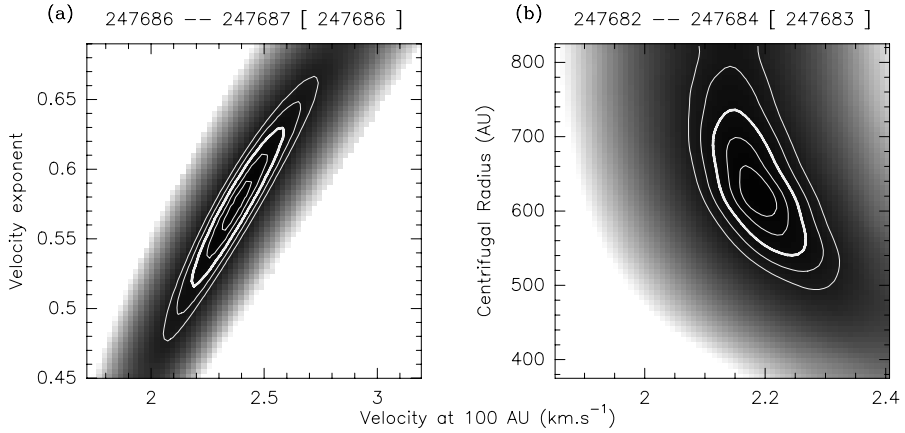

Fig. 8. a Rotation velocity V_0 as a function of exponent v. **b** Rotation velocity as a function of centrifugal radius R_c. The rotation velocity was assumed to fall as r^{-1} beyond the centrifugal radius. Contours are 1 to 5σ, with the 3σ level enhanced.

hence $M \propto D^{0.5-0.75}$), but also depends on uncertainty in the spectral type.

Rotating Keplerian disks have now been discovered around an increasing number of PMS stars: the binary system GG Tau (DGS94), GM Aur (Koerner et al 1993, Dutrey et al 1998), MWC 480 (Mannings et al 1997), DM Tau (this work). Our method can be used to provide the stellar mass independently of the stellar properties and theoretical evolutionary tracks. It is however important to understand the main limitations on the accuracy of the method. The error on the mass is given by

$$\frac{dM}{M} = 2\frac{dV_0}{V_0} + \frac{dD}{D} \quad (5)$$

and, to first order, the error on the rotation velocity is dominated by the error on the inclination:

$$\frac{dM}{M} = 2\frac{\cos(i)}{\sin(i)}di + \frac{dD}{D} \quad (6)$$

Although our method provides simultaneous determinations of the inclination i and rotation velocity V_0, any independent measurement of the inclination i will help in reducing the uncertainty in the mass determination. Furthermore, the most inclined disks will provide better stellar mass estimates: the accuracy obtained for a disk tilted by $70 \pm 10°$ is similar (13 %) to that obtained for DM Tau, where $i = 33 \pm 3°$. Higher angular resolution images could provide more accurate results. The distance uncertainty will then become the dominant error. Unfortunately, the precision of the Taurus distance determination from the Hipparcos mission is still about 10 %.

6.3. Analysis from integrated spectra

While CO images from protoplanetary disks are becoming available, detection of molecules other than CO have so far been performed only with large single-dish telescopes (DGG97, Kastner et al 1997). In this case, one is forced to use the integrated spectra to derive physical parameters of the disk. The disk properties discussed in Sect. 4.1 can be used to derive approximate disk parameters in such a case.

When only integrated spectra are available, parameter ρ introduced in Eq. 2 is essential to derive disk sizes and/or tem-

peratures. This approach was used by DGG97 for the analysis of molecular abundances in DM Tau and GG Tau. Fig. 4 shows the value of ρ and $\rho\Delta V$ as a function of opacity at 500 AU τ. The opacity is defined as the opacity perpendicular to the disk:

$$\tau(r) = \kappa(r)\Sigma(r)/\Delta V \quad (7)$$

where $\kappa(r)$ is the line absorption coefficient. The value of $\rho\Delta V = 0.3$ used by DGG97 is outlined by the dashed lines in Fig. 4; it is valid for moderately optically thick lines, corresponding to $\tau = 2.9$ at $R = 500$ AU. As such, it is a reasonable value to use to determine minimal outer radii for spectral lines which are unlikely to be extremely optically thick. This result justifies the values given by DGG97 in their Table 2. One exception is ^{12}CO, which potentially has much higher optical depths: a higher value should be used for ρ, and hence a lower value of the outer radius will be found. To some extent, HCO^+ could have been affected by a similar effect, but the lack of detection of the $H^{13}CO^+$ isotopomer indicates that the opacity of the HCO^+ J $= 1 \rightarrow 0$ line is less than $\simeq 4$, consistent with a value of $\rho\Delta V = 0.3$.

7. Conclusions

We have resolved the circumstellar disk of DM Tau in the ^{12}CO J $= 1 \rightarrow 0$ line, showing unambiguously that the disk rotates around the central star. The disk is inclined 33° from the plane of the sky, and self-absorption effects show that the disk must be flared, with the Western part towards us. We developed a general χ^2 fitting technique to further derive physical parameters of the disk using a standard disk model in hydrostatic equilibrium. We evaluated the dependencies between the various disk parameters due to the disk properties, and show that a 5 parameter global fit including $(T_0, q, V_0, i, R_{\rm out})$ is required for a proper evaluation of the parameter error bars.

Applying this method to DM Tau, we show that the rotation pattern is consistent with Keplerian rotation, and derive an accurate mass for the central star, $M = 0.50 \pm 0.06\,{\rm M}_\odot (D/150\,{\rm pc})$, i.e. $M = 0.50 \pm 0.11\,{\rm M}_\odot$ if a 10% error on the distance is included. Because the ^{12}CO J $= 1 \rightarrow 0$ line is optically thick, the disk size and temperature can also be derived. The outer radius of the disk is quite large (850 AU). Such large gas disks seem to be a common feature, and have been found around an increasing number of pre main sequence stars, singles (e.g. GM Aur, Dutrey et al 1998, MWC 480, Mannings et al 1997) as well as binaries (GG Tau, DGS94, UY Aur, Duvert et al 1998).

The temperature law is well constrained, and consistent with stellar heating in a flared disk. On the other hand, the density law cannot be determined from these observations. The kinematic pattern indicates that the turbulence in the disk must be small, of order $\sim$ 0.2–0.3 times the thermal width, or about $0.1\,{\rm km\,s^{-1}}$, although the exact value depends on the assumed density. More precise values for density and line width would require the observation of an optically thin line, e.g. ^{13}CO, to sample the density profile. Then, all the disk parameters could be caracterized. We caution, however, that because of sensitivity limitations of the current millimeter arrays, such studies are only relevant to the outer parts of the disk, for $r > 60$–100 AU.

Acknowledgements. This work would not have been possible without the special effort of the IRAM backend group to implement a high spectral resolution mode on the Plateau de Bure correlator. We also thank G.Duvert, M.Guélin and K.Schuster for fruitful discussions.

References

Beckwith, S.V.W., Sargent, A.I, Chini, R.S., and Güsten, R., 1990, AJ, 99, 924
Beckwith, S.V.W., and Sargent, A.I, 1993, ApJ 402, 280
Cabrit, S., Guilloteau, S., André, P. et al., 1996, A & A, 305, 527
Dutrey, A., Guilloteau, S., Simon, M. 1994, A&A 286, 149 (DGS94)
Dutrey, A., Guilloteau, S., Duvert, G., Prato, L., Simon, M., Schuster, K., Ménard, F. 1996, A&A 309, 493
Dutrey, A., Guilloteau, S., Guélin, M. 1997, A&A, 317, L55 (DGG97)
Dutrey, A., Guilloteau, S., Prato et al., 1998, A&A Letters, in press
Duvert, G., Dutrey, A., Guilloteau, S. et al., 1998, A&A 332, 867
Gueth, F., Guilloteau, S., Dutrey, A., Bachiller, R., A&A, 323, 943
Guilloteau, S., Dutrey, A., 1994, A&A 291, L23 (GD94)
Hayashi, M., Ohashi, N., and Miyama, S., 1993, ApJ 418, L71
Kastner, J.H., Zuckerman, B., Weintraub, D.A., Forveille, T., 1997, Science 277, 67
Koerner, D.W., Sargent A.I., Beckwith S.V.W., 1993, Icarus 106, 2
Koerner, D.W., Sargent A.I., 1995, AJ 109, 2138
Mannings, V., Koerner D.W., Sargent, A.I., 1997, Nature 388, 555
Mazitelli, I. 1989, in *Low Mass Star Formation and Pre-Main Sequence Objects*, B. Reipurth, ed., ESO Proc. No.33.
Myers, P.C., Bachiller, R., Caselli, P. et al., 1995, ApJ 449, L65
Saito, M., Kawabe, R., Ishiguro, M. et al., 1995, ApJ 453, 384
Sargent, A.I., and Beckwith, S.V.W., 1991, ApJ 382, L31
Zhou, S., Evans, N.J., Koempe, C., Walmsley, C.M., 1993, ApJ 404, 232